Data-Driven Simulations of the Lightning Return Stroke Channel Properties

Michael C. Taylor, Caitano L. da Silva, T. Daniel Walker, and Hugh J. Christian

***Abstract*—Accurate estimates of the lightning channel plasma properties are crucial for quantifying the impacts of lightning in the atmosphere and on man-made structures. Gas dynamics models of the return stroke help provide a fundamental understanding of the transformation that occurs in an air parcel subject to the lightning current, yielding quantitative estimates of important channel properties, such as its radius, temperature, and energy deposition. However, until very recently, there was no dataset available in the literature that permitted proper validation of such simulation techniques. This knowledge gap was closed recently when high-speed optical spectra of triggered lightning were made available. In this article, we use measurements to drive and constrain simulations with a gas dynamic model. The model employs a number of parameterizations that allow us to rewrite the hydrodynamic problem as a set of ordinary differential equations. Comparisons with measured temperature and electron density yield errors of the order of tens of percent. The use of more accurate air-plasma transport coefficients helps improve the agreement with measurements. Additionally, we estimate key channel parameters that are not easily measured. The calculated channel radius, resistance, and deposited energy agree well with what has been previously reported in the literature.**

***Index Terms*—Lightning electromagnetic pulse (LEMP), lightning, lightning measurement, modeling.**

I. Introduction

WHEN lightning leader channels connect to a ground structure, a powerful surge travels upward into the cloud. Lightning leaders are filamentary plasma channels that carve the way for lightning to come from cloud to ground. The return stroke is an intense nonlinear ionization wave, which transforms the leader channel into a hot and highly-conducting plasma [1], with temperatures and electron densities in excess of 30 000 K and 10^{24} m^{-3}, respectively [2], [3]. The return stroke is the glare on the horizon one sees with the naked eye when a lightning flash occurs nearby. The glare is evidence of electrical energy stored in the clouds being converted into optical radiation as the lightning channel current excites, ionizes, and dissociates air molecules. The return stroke also converts electrical energy into radiation in other bands of the optical spectrum, acoustic radiation (making thunder), and radio waves (which allow long-distance detection and location of lightning flashes).

The lightning return stroke is the most widely studied aspect of a lightning flash due to its impacts on the atmosphere and deleterious effects to man-made structures [4]. Accurate estimates of the lightning return stroke channel properties, such as temperature, conductivity, radius, resistance, and energy deposition (magnitude and rate), are critical for quantifying the impacts of lightning. For instance, temperature and radius are crucial for estimating nitrogen oxide yields by lightning [5]. Similarly, resistance is crucial for determining the height-dependent current flow in the channel, which in its turn determines the radiated electric fields [6]. These electric fields should be calculated with precision to quantify lightning-induced voltages in power transmission and distribution systems [7]. As a final example, accurate understanding of energy deposition rates can help quantify thermal and mechanical impacts of lightning on aircrafts [8].

Computational models that aim to simulate the lightning return stroke and shed some light on the observed features can be divided into four different categories: 1) gas dynamic, 2) electromagnetic, 3) distributed-circuit, and 4) engineering models [9]. The first category contains the models devised to calculate the return stroke channel properties, such as the one employed in this article. We will not review the other categories as they are beyond the scope of this article. Gas dynamic models describe the evolution of key parameters in a short segment of the lightning channel by solving hydrodynamic equations associated with the conservation of energy, mass, and momentum [10], [11]. The seminal work of Plooster [10] attempted to compare their calculations with experimental measurements available at the time [12]–[14]. Plooster's calculations provided reasonable agreement with the temperature measured by Orville [13], and consequently, that work has served as a benchmark for all other gas dynamic models that have been published since. The caveat is that no other information about the return stroke was known to allow the author to constrain the calculations. This issue has persisted for nearly 50 years until Walker and Christian [2], [3] published the first high-speed optical spectra of lightning accompanied by channel base current measurements. Addressing this issue is the primary goal of this article.

The objective of this work is to simulate the lightning return stroke channel plasma constrained by the measurements made

Manuscript received 4 April 2022; revised 24 May 2022 and 20 June 2022; accepted 28 June 2022. This work was supported by the NSF under Grant AGS-1917069 and Grant AGS-2046043 (CAREER) to New Mexico Tech (NMT) and by the NSF EPSCoR Program under Award OIA-1757207 (as a subaward made to NMT). *(Corresponding author: Caitano L. da Silva.)*

Michael C. Taylor and Caitano L. da Silva are with the Department of Physics and Langmuir Laboratory, New Mexico Institute of Mining and Technology, Socorro, NM 87801 USA (e-mail: michael.taylor@student.nmt.edu; caitano.dasilva@gmail.com).

T. Daniel Walker and Hugh J. Christian are with the Earth System Science Center, The University of Alabama in Huntsville, Huntsville, AL 35899 USA (e-mail: walkertd@uah.edu; christian@nsstc.uah.edu).

Color versions of one or more figures in this article are available at https://doi.org/10.1109/TEMC.2022.3189590.

Digital Object Identifier 10.1109/TEMC.2022.3189590

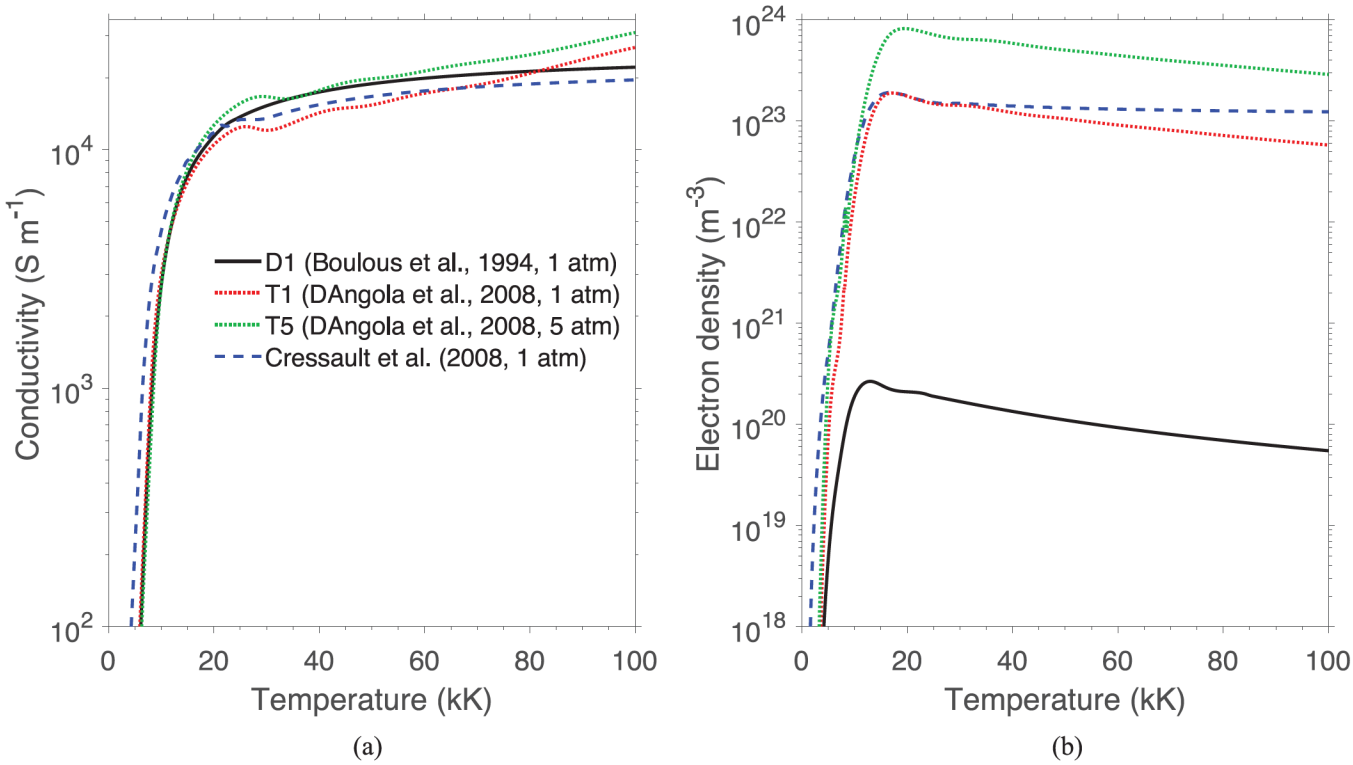

Fig. 1. (a) LTE electronic conductivity and (b) electron density as a function of temperature. The legend specifies three model cases used in this article, as well as their corresponding atmospheric pressures.

by Walker and Christian [3]. The model, described in da Silva *et al.* [1], is driven by the actual channel base current and the initial conditions are adjusted to best match the measured electron density and temperature. This dataset allows, for the first time, for a gas dynamic model to be properly tested. After obtaining reasonable agreement between the model and observations, we proceed to use the model to estimate key return stroke channel parameters that cannot be easily measured, such as radius, resistance, energy deposition, electric field, and more.

II. Methods

A. Model for the Lightning Return Stroke Channel Properties

In this work, we simulate the lightning return stroke channel properties with the model proposed by da Silva *et al.* [1]. It is based on the gas dynamic or physical models of the lightning return stroke [9]. The model assumes that the lightning channel is axially symmetric and that its (axial) length is much larger than the radius. This allows the relevant problem to be written as a series of ordinary differential equations. Some of the key assumptions that describe the model's underlying physics include the following.

1) The current is determined externally and simply imposed on the channel section of interest.
2) The radial profile of the relevant plasma properties (e.g., temperature) may be represented by two parameters only, the average value inside of the channel and its radius.
3) Rates of thermal ionization are parameterized in such a way that at very high temperatures ($\gtrsim$10 kK), the model must converge to the well-known local thermodynamic equilibrium (LTE) properties of an air plasma.

The latter is done by imposing that the rate of associative ionization must be proportional to the LTE electron density n_{LTE} at the temperature of interest. In this model, the radial profile of the channel's plasma density and temperature has the shape of a top-hat function, as shown in [1, Fig. 1(c)]. The channel expands mostly driven by ambipolar diffusion, and the calculated radial growth as a function of time can be seen in [1, Fig. 6(d)], for a typical return stroke simulation.

In [1], the LTE coefficients from Boulos *et al.* [15] are used. The corresponding LTE conductivity σ_{LTE} is shown in Fig. 1(a). Boulos *et al.* [15] do not provide calculations of the LTE electron density, and for this reason, the electron density was approximated as $n_{\mathrm{LTE}} = \sigma_{\mathrm{LTE}}/e\mu_e$, where e and μ_e are the electronic charge and mobility, respectively. This approximation ensures that at high temperatures, the correct conductivity is obtained. The resulting n_{LTE} is shown in Fig. 1(b). In this work, we extend the model [1] to use a more comprehensive set of LTE coefficients provided by D'Angola *et al.* [16] as a series of interpolation formulas to their first-principles calculations. D'Angola *et al.*'s coefficients agree very well with independent calculations by Cressault *et al.* [17], as can be seen in Fig. 1. However, it is easy to see that the LTE electron density used in [1] is about 3 orders of magnitude lower than the other two references [see Fig. 1(b)]. Another advantage of using D'Angola

et al.'s coefficients is that their calculations were made for a number of different pressures. It can be seen from Fig. 1 that increasing the channel pressure from 1 to 5 atm increases the electron density [see Fig. 1(b)], but it does not change the conductivity very much [see Fig. 1(a)]. Hereafter, we refer to three different model *cases*, which correspond to the usage of the different coefficients shown in Fig. 1. They are as follows.

- D1: An identical replica of the model used in da Silva *et al.* [1], with the LTE conductivity from the work in [15].
- T1: The primary improvement proposed in this work, which replaces the LTE electron density with the calculations of D'Angola *et al.* [16].
- T5: Same as T1, but the average pressure inside of the channel is increased from 1 to 5 atm.

The electronic mobility given above is defined as $\mu_e = e/m_e(\nu_{eN} + \nu_{ei})$, where ν_{eN} and ν_{ei} are the frequency of collisions between electrons and neutral species and between electrons and ions, respectively, and m_e is the electron mass. The 2019 version of the model simply assumed that the collisions with neutral particles are dominant and, thus, had $\nu_{ei} = 0$ and ν_{eN} given according to Cho and Rycroft [18]. In this work, we include electron–ion collisions with $\nu_{ei} \propto n/T_e^{3/2}$ given according to Chernyi *et al.* [19], where T_e is the electronic temperature and n is the plasma density (the population of electrons and ions is assumed to be approximately balanced). The inclusion of ν_{ei} helps ensure that at high temperatures, the conductivity is only a function of temperature, and not of electron density (as it is at low temperatures) [20].

B. Constraining Simulations With Observations

In this article, we use data from a triggered lightning flash collected at the International Center for Lightning Research and Testing (ICLRT) in Camp Blanding, FL, USA. The triggered flash took place on August 1, 2013, at 19:25:35 UTC. It is designated as UF 13-27 in the ICLRT archives [21], [22]. A total of five return strokes were observed with an average rise time of 3.2 μs. Measured peak currents were 15.3, 9.3, 13.5, 17.3, and 8.1 kA, in this order. The interstroke intervals were 88, 29, 107, and 186 ms, respectively.

Simultaneously to the channel-base current measurements, Walker and Christian [2], [3] recorded the discharges' optical spectrum with 1.5-μs temporal resolution. These authors achieved high temporal resolution by mounting a grism in front of a Phantom V710 high-speed camera. A grism is a combination of a diffraction grating and a prism. Particularly in this case, the system consisted of a set of volume-phase holographic grisms, constructed using dichromated gel, encapsulated between two prisms [2]. The Phantom V710 camera imaged a 1-m channel segment located around 50 m above ground level. The recorded spectra consisted of two major regions of interest: soft ultraviolet to visible (320–620 nm) and visible to near-infrared (620–870 nm). Using the relative magnitude of neutral and singly-ionized lines of nitrogen and hydrogen, these authors infer the temporal evolution of electron density and temperature for the five return strokes listed above [3].

In this article, we drive our simulations with the precise channel-base current reported by Walker and Christian [3], and then, we compare the calculated temperature (T) and electron density (n) with Walker and Christian's estimates. The initial conditions of the model, namely the initial channel radius and temperature, are adjusted until the best match between simulations and measurements is obtained. The temperature error (δT) between simulation and measurements is calculated in % as

$$\delta T = \left\langle \left| \frac{T_i^{\rm sim} - T_i^{\rm data}}{T_i^{\rm data}} \right| \right\rangle , \tag{1}$$

where T_i are evaluated for all points in the measurement time series. A similar expression defines the error in electron density calculations (δn). A combined error (CE) can give an idea of how the model can capture the evolution of both T and n simultaneously. The CE is given as

$$\mathrm{CE} \equiv \delta T n = \sqrt{\delta T^2 + \delta n^2} \, . \tag{2}$$

In Section III, we discuss how it is typically more difficult to match the measured electron density, rather than the temperature. Therefore, δn typically dominates the error estimates in equation (2). For this reason, when finding the set of initial conditions that yields the best agreement between simulations and model, we use a normalized CE (NCE) defined according to the following expression:

$$\mathrm{NCE}^2 = \left[\frac{\delta T - \min(\delta T)}{\max(\delta T) - \min(\delta T)} \right]^2 + \left[\frac{\delta n - \min(\delta n)}{\max(\delta n) - \min(\delta n)} \right]^2 . \tag{3}$$

We perform a series of simulations varying the initial channel radius between 0.1 and 10 mm, and the initial temperature between 300 and 1300 K. The maximum and minimum errors are determined, $\max(T)$ and $\min(T)$, respectively. These errors are fed into (3) for normalization purposes. Fig. 2 illustrates, among other things, how the best fit is found. The top and bottom rows in the figure show information about temperature and electron density calculations, respectively. All panels are given as a function of the initial channel radius. The different curves indicate different initial temperatures. Fig. 2(a) and (d) shows the average temperature and electron density, according to (1), respectively. It can be seen from these figures that, for the fifth stroke in this flash, the minimal average temperature error is 22% while the lowest average electron density error is 69%, over three times larger. The simulations shown in Fig. 2 were performed with the T1 variation of the model. The best fit, marked with a circle in the figure, is selected by minimizing the results of (3). An initial set of simulations is performed by varying the initial channel radius between 0.1 and 10 mm in increments of 1 mm, and the initial temperature between 300 and 1300 K in increments of 200 K. After the best fit is found, we reduce the extent of the parametric space by centering in the best fit found $\pm$1 mm and $\pm$200 K. This refinement is repeated a second time (now reducing the increments of initial radius and temperature to 0.1 mm and 50 K, respectively) until we find the

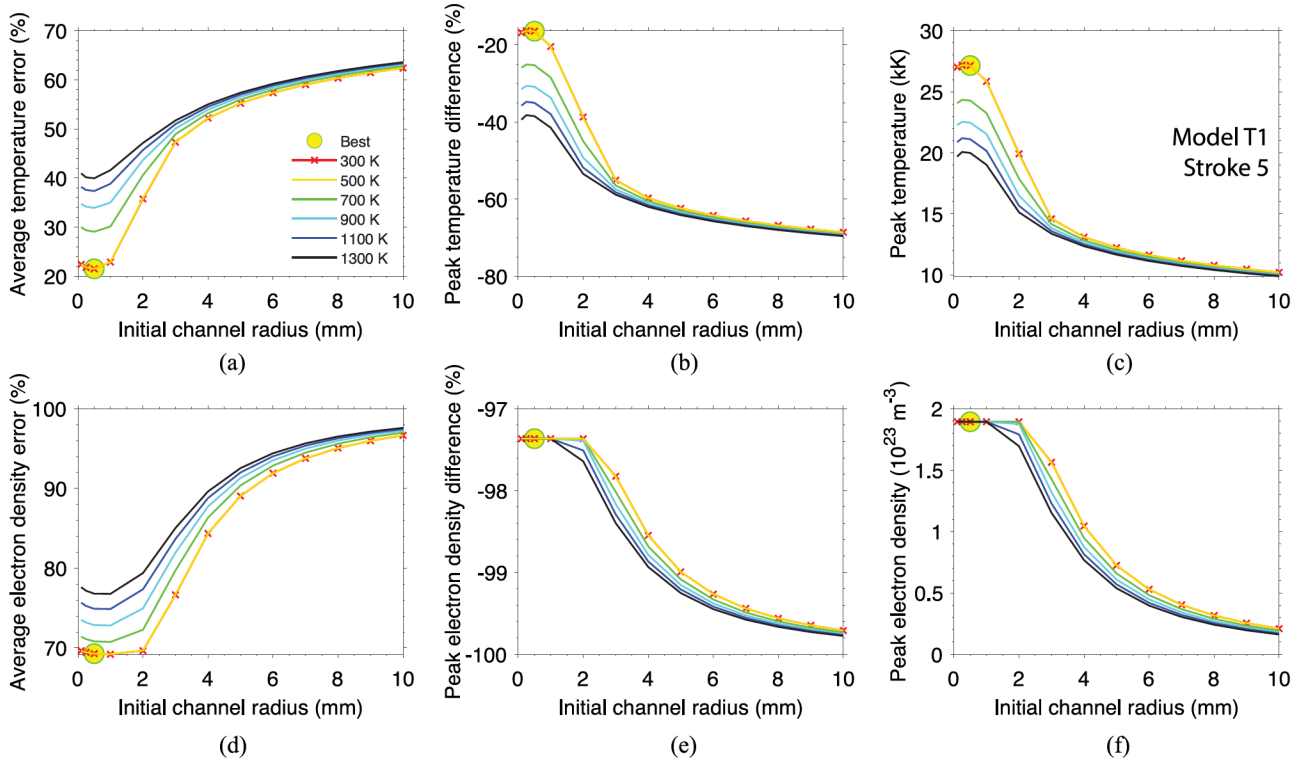

Fig. 2. Parametric search to determine the set of initial conditions that allows the model to best fit the data. Panels (a), (b), (d), and (e) show different error metrics between the simulation and data with (a)–(c) corresponding to the temperature and (d)–(f) to the electron density. The six panels show (a) average temperature error, (b) difference in peak temperature, (c) simulated peak temperature, (d) average electron density error, (e) difference in peak electron density, and (f) simulated peak electron density. The set of initial parameters that yields minimal NCE is marked with a yellow circle.

initial conditions that make model and measurements agree with minimal NCE.

We would like to conclude this section by emphasizing that the deviation between model and measurements, of the order of tens of percent, is obtained when driving the simulations with the actual current flowing through the triggered lightning channel. This level of constraint yields higher confidence in the model results, something that Plooster [10] and all subsequent works could not provide, simply due to the lack of proper ground truth data in the literature for comparison.

III. Results

In the previous section, we outlined the method to match simulations and measurements. The technique is illustrated in Fig. 2 for the fifth stroke of the flash under consideration and for model case T1. Figs. 2(a) and (d) show the calculated fit error, given as in (1), for several initial conditions. Fig. 2(b) and (e) show that the model underestimates both the measured peak electron density and peak temperature (note the negative % difference in both figures). This is actually consistent across all simulations reported in this article. Fig. 2(c) shows that the calculated peak temperature is inversely proportional to the initial radius and initial temperature. This proportionality rule also applies to the calculated peak electron density, as shown in Fig. 2(f). All panels in Fig. 2 show that the calculations are more sensitive to the initial radius, rather than the temperature. All five strokes in the triggered lightning flash UF 13-27 were matched to the three different variations of the model used, cases D1, T1, and T5. The initial conditions that best fit all cases are listed in Section A of Table I, as well as the resulting fitting errors (see Section B).

Fig. 3 shows the temporal dynamics of the primary return stroke channel properties of interest, corresponding to the first [top row, Fig. 3(a)–(c)] and fifth [bottom row, Fig. 3(d)–(f)] strokes in the triggered flash. Figs. 3(a) and (d) show the measured channel-base current that drives the simulations. Fig. 3(b) and (e) show the simulated temperature using the three different model variations and comparison to measurements. Figs. 3(c) and (f) show the same for the electron density. It can be seen that the original model from the work in [1], marked as D1, can capture very well the high temperatures measured (middle column in the figure). It can also be seen that the proposed improvement in this work, of replacing the LTE coefficients from Boulos *et al.* [15] with the ones given by D'Angola *et al.* [16], labeled as case T1, increases the calculated electron density by more than one order of magnitude, improving the agreement with measurements (rightmost column). The best agreement with the electron density inferred by Walker and Christian [3] is obtained when we increase the atmospheric pressure inside of the channel to 5 atm, as can be seen in Figs. 3(c) and (f) (model case T5). This new model feature (T5 in the figure) is only possible because D'Angola *et al.* [16] provide the LTE electron density calculated at several different pressures. All model variations capture well the rate of channel cooling right after the return stroke peak current, which is 1.6 kK/μs averaged over the five strikes.

TABLE I

SUMMARY OF ALL SIMULATION RESULTS, INCLUDING (ACROSS THE ROWS) STROKE PROPERTIES, ERROR METRICS, AND EXTRACTED CHANNEL PROPERTIES, FOR THE FIVE STROKES (IN THE DIFFERENT COLUMNS)

Stroke Number	1			2			3			4			5			Average			Standard Deviation		
Model name	D1	T1	T5	D1	T1	T5	D1	T1	T5	D1	T1	T5	D1	T1	T5	D1	T1	T5	D1	T1	T5
Model generation	2019	This work		2019	This work		2019	This work		2019	This work		2019	This work		2019	This work		2019	This work	
Atmospheric pressure (atm)	1	1	5	1	1	5	1	1	5	1	1	5	1	1	5	1	1	5	1	1	5
A. Stroke properties																					
Peak current (kA)		15.4			9.3			13.4			17.3			8.1			12.7			3.93	
Risetime (μs)		3.3			3			3.5			3.3			3			3.2			0.21	
FWHM (μs)		46			39			46			45			32			42			6.2	
Initial radius (mm)	0.1	0.4	0.2	0.3	0.7	0.1	0.2	0.4	0.2	0.1	0.4	0.2	0.1	0.5	0.2	0.16	0.48	0.18	0.09	0.13	0.04
Initial temperature (K)	650	450	550	400	500	500	450	300	300	550	450	300	550	300	300	520	400	390	97	94	124
B. Error characterization																					
Average T error (%)	15	11	22	5.4	24	35	8.1	18	30	17	18	28	3.1	22	32	9.8	19	29	6.1	4.9	5.0
Average n error (%)	98	70	56	98	69	50	98	70	56	98	70	55	99	69	50	98	70	53	0.17	0.60	3
Combined error (%)	99.43	71.34	60	98	73	61	98	72	64	100	72	61.2	99	73	59	99	72	61	0.59	0.64	1.7
Measured peak T (kK)		34			35			35			43			33			36			3.8	
Calculated peak T (kK)	33	31	25	34	28	23	35	30	25	36	32	27	32	27	23	34	30	24	1.6	2.1	1.6
Measured peak n (10^{23} m^{-3})		72			83			85			620			48			180			250	
Calculated peak n (10^{23} m^{-3})	.21	1.9	8.2	.19	1.9	8.2	.22	1.9	8.2	.25	1.9	8.2	.17	1.9	8.2	.21	1.9	8.2	.30	0.0	0.0
C. Extracted Properties at Instant of Peak Power																					
Peak dissipated power (MW/m)	160	41	9.6	110	20	5.0	170	33	8.3	200	47	13	91	16	3.7	150	31	7.9	44	13	3.6
Radius (mm)	3.70	1.9	1.5	3.0	1.7	1.2	3.4	1.9	1.4	3.5	2.0	1.5	2.8	1.6	1.2	3.3	1.8	1.4	0.40	0.20	0.15
Conductivity (10^4 S/m)	3.3	39	290	2.6	39	280	2.8	39	270	3.6	39	260	2.6	39	290	3.0	39	280	0.46	0.090	14
Resistance (Ω/m)	0.72	0.22	0.051	1.4	0.29	0.080	0.95	0.22	0.060	0.70	0.20	0.057	1.6	0.33	0.079	1.1	0.25	0.070	0.41	0.060	0.010
Electric field (kV/m)	11	3.0	0.70	13	2.4	0.63	13	2.7	0.71	12	3.0	0.85	12	2.3	0.54	12	2.7	0.68	0.76	0.34	0.11
D. Extracted Properties at 100 μs																					
Charge transferred (C)		0.83			0.45			0.71			0.91			0.35			0.67			0.21	
Dissipated energy (J/m)	6200	1300	750	3400	740	560	5700	920	560	7400	1500	1000	2600	720	580	5100	1000	690	2000	340	190
Radius (mm)	8.0	4.4	3.8	6.4	3.9	3.3	7.2	4.3	3.6	7.8	4.5	3.8	6.1	3.7	3.2	7.1	4.2	3.5	0.85	0.36	0.27
Conductivity (10^4 S/m)	0.56	9.0	21	0.48	5.8	12	0.53	7.0	16	0.63	10	24	0.47	5.6	12	0.53	7.6	17	0.070	2.1	5.4
Resistance (Ω/m)	0.90	0.18	0.11	1.6	0.37	0.24	1.2	0.25	0.15	0.82	0.15	0.093	1.8	0.42	0.27	1.3	0.27	0.17	0.45	0.12	0.080
Electric field (kV/m)	3.9	0.80	0.47	3.5	0.77	0.51	3.7	0.80	0.49	4.3	0.79	0.48	3.5	0.79	0.51	3.8	0.79	0.49	0.34	0.010	0.020

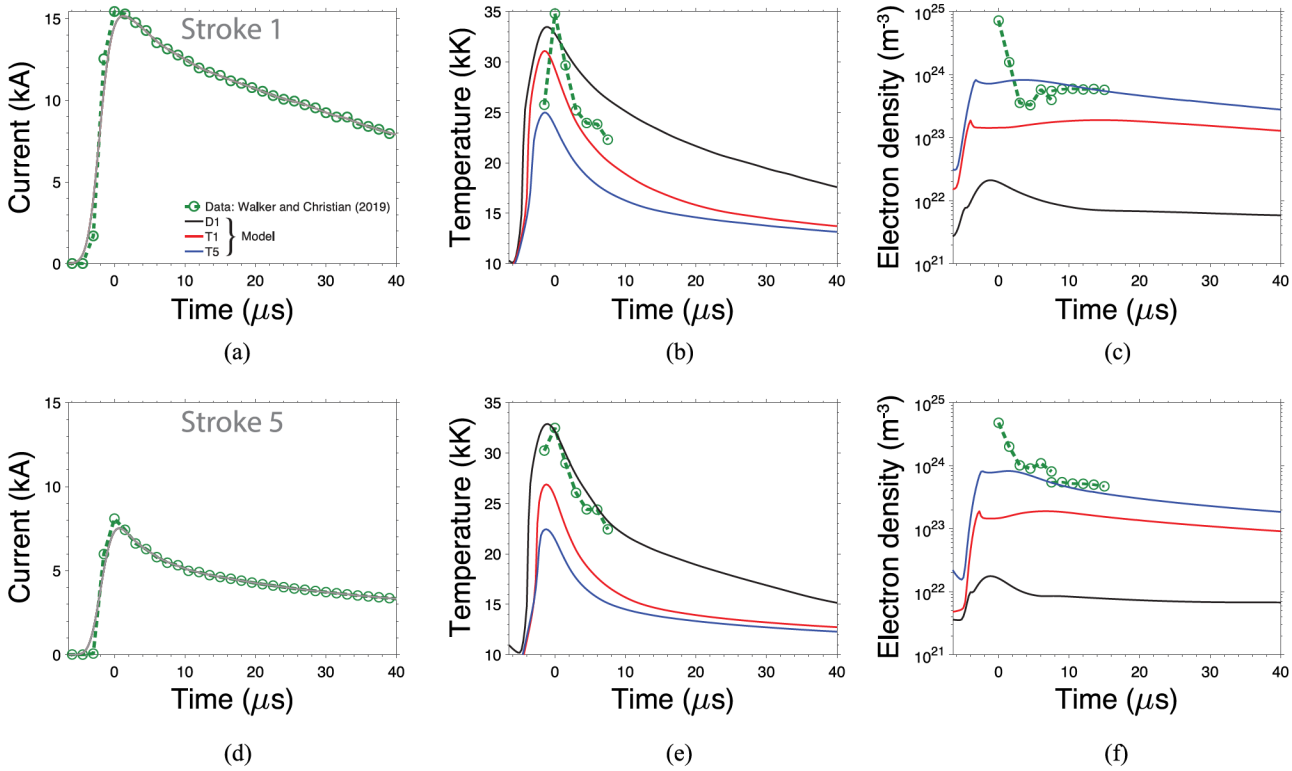

Fig. 3. Simulation of the first (a)–(c) and fifth (d)–(f) return strokes in the UF 13-27 triggered lightning flash. (a) and (d) Channel-base current that drives the simulations. (b) and (e) Comparison between simulated and measured temperature. (c) and (f) Comparison between simulated and measured electron density. The different curves show simulation results from the three model cases employed.

Fig. 3 illustrates the fundamental physical limitations of the model. For all different configurations used, it is essentially impossible to capture high temperatures and plasma densities simultaneously. This happens because these two quantities are essentially inversely proportional in a computer simulation driven by an external current. This happens because the heating rate ($\partial T/\partial t$) is proportional to I^2/n, where I is the imposed electrical current. Nonetheless, the results in Fig. 3 present, for the first time, reasonable quantitative agreement between a computer simulation and measured lightning channel plasma properties. Table I shows that the simulations capture very well the high temperatures measured, with typical reproduction errors between 10% and 29% across the three model cases. On the other hand, the three model cases struggle to yield the high electron densities measured. The values derived from cases T1 and T5 are, nonetheless, comparable to what has been previously reported in the literature, of the order of 10^{23}–10^{24} m^{-3} [13].

Table I shows detailed simulation results for all five strikes. For each of the five strikes, results are presented for the three different model cases. The table has four main sections. Section A shows the main stroke properties extracted from the current waveform, as well as the initial conditions (radius and temperature) that lead to the best fit between the model and observations. Section B lists the key error metrics and parameters involved in error calculation. Section C reports on inferred channel properties at the instant of peak electrical power (or peak current), whereas Section D shows similar properties extracted 100 μs after peak current.

The last six columns in Table I show average and standard deviation across the five strikes for the three different model cases. At the instant of peak current, the mean values for peak dissipated power vary between 7.9 and 150 MW/m. Similarly, the calculated channel resistance for this same instant varies between 0.07 and 1.1 Ω/m. These values are about one order of magnitude lower than the ones provided by Jayakumar *et al.* [23], who reported 220–2510 MW/m and 0.67–31 Ω/m. On the other hand, our radius estimates at the instant of peak power, 1.4–3.3 mm, produce better agreement with Jayakumar *et al.* [23], who reported values in the range of 1.0–6.9 mm. The dissipated energy up to 100 μs, amounting to 0.7–5.1 kJ/m also agrees well with estimates available in the literature. Typical numbers are of the order of 1–10 kJ/m, as reported in Table I of Rakov and Uman [9]. For specific comparison, Jayakumar *et al.* [23] report values in the range of 0.9–6.4 kJ/m. It should be noted that the measurements that constrain our calculations [2], [3] correspond to a 1-m section of the channel about 50 m above ground level, but for the sake of simplicity, we have used the current measured at the channel base to drive the simulations. The current attenuation as it travels upward through the channel should somehow affect the energy estimates reported here, as discussed by Cooray [24]. In order to alleviate these uncertainties, we report below parameter estimates for a range of current values.

There are two primary sources of variation in the parameter estimates given in Sections C and D of Table I: 1) the choice among the three model cases used, and 2) the stroke peak current. Fig. 4

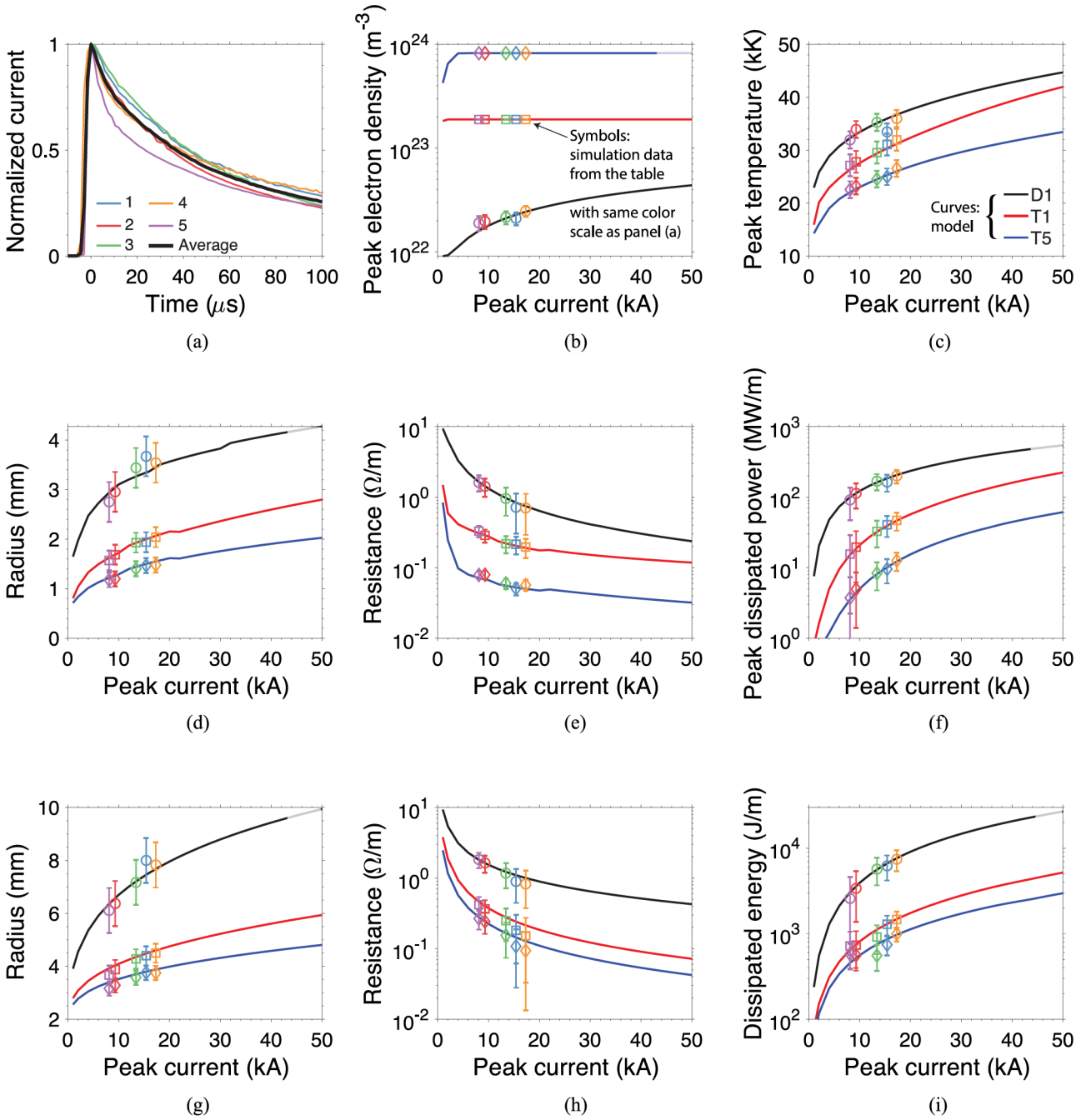

Fig. 4. (a) Normalized current waveforms, and (b)–(i) calculated return stroke channel properties as a function of peak current. (b) and (c) Peak electron density and temperature, (d)–(f) key extracted properties at the instant of peak power, and (g)–(i) 100 μs later. Simulations are driven with the average current waveform shown in panel (a) and with average initial conditions for radius (= 0.27 mm) and temperature (= 437 K). The only varying quantity is peak current. The curves show simulations with the three different model cases used while the symbols show the results reported in Table I (with unique initial conditions). Error bars correspond to the standard deviation across the five strikes. Note that plots with log scale distort the error bars.

is constructed to provide a correction for the latter dependence. Fig. 4(a) shows that the current waveform for the five return strokes studied is relatively similar to each other. We proceed to average the current waveform [black curve in Fig. 4(a)] and the initial conditions that best match the simulations (radius = 0.27 mm and temperature = 437 K) and to perform a number of simulations varying only the return stroke peak current. The results are shown in the subsequent panels in Fig. 4. The curves show the calculations for the three different model cases while the symbols show the actual values reported in Table I. It can be seen that peak electron density [see Fig. 4(b)] does not increase with peak current. This happens because the LTE electron density has little dependence on temperature beyond 20 kK, as shown in Fig. 1(b). This result indicates that electron density may not be an ideal quantity to use as a means of retrieving other parameters from the lightning return stroke channel, because it is

fairly insensitive to the driving conditions. Contrastingly, peak temperature [see Fig. 4(c)] has a clear correlation with peak current.

The next two rows show parameters extracted at the instant of peak power [see Fig. 4(d)–(f)], and 100 μs later [see Fig. 4(g)–(i)]. All parameters reported have a clear dependence on peak current. Nonetheless, the primary source of variation in the estimates arises from the different model case selections. When using the results reported in Fig. 4, we recommend the reader proceeds in the following manner. First, use the results from the T1 case as data-constrained estimates of the return stroke channel properties, since this case does the best job of simultaneously reproducing the measured electron density and temperature. Second, use the results of D1 and T5 model variations as an order-of-magnitude confidence interval around the estimate. For instance, one could say that the data-constrained calculations predict that a 10-kA return stroke dissipates 800 J/m in the first 100 μs of its lifetime, and with greater confidence, one could say that the energy dissipated lies in between the 500 and 4000 J/m figures.

Finally, we conclude this section with a discussion of memory effects. If we look exclusively at the measured data, the peak temperature and electron density do not show any evidence of memory effects, i.e., they do not correlate with stroke order, or with interstroke interval. They do not even correlate with peak current very well for that matter. Strokes 1, 2, 3, and 5 all have comparable temperatures and electron densities, of about 34 kK and 7.2×10^{24} m^{-3}, respectively. However, stroke 4 stands out as having the highest peak current (50% larger), temperature (25% larger), and electron density (8 times larger). The only evidence of memory effects arises when we cross-reference the return stroke peak current with the interstroke interval that follows it. The four interstroke intervals reported can be approximately predicted according to the formula $\Delta t = 17I_p - 133$, where Δt is given in milliseconds and the peak current I_p is given in kiloamperes. The coefficient of determination between Δt and I_p is $R^2 = 0.8$. The typical error arising from using this fit formula is about 20%. The peak temperature and electron density of a stroke, on the other hand, are not good predictors of the interstroke interval that follows.

Additional evidence for the lack of memory effects arises from the fact that all five return strokes were fitted with similar initial conditions resembling a prebreakdown channel, i.e., with a narrow radius (of about 3 mm) and with a low temperature (of about 400 K). This result suggests that interstroke intervals as low as 30 ms are sufficient for the channel to substantially cool down to near-ambient conditions. Even though the channel cools down, it remains a more favorable path for dart leaders to create subsequent return strokes. Beyond high-temperature and plasma density, channel conditioning can manifest itself in a number of other ways, such as reduced air density and increased ion concentration (inside of the channel with respect to ambient atmospheric air), for example. Our conclusions that the inferred initial conditions resemble a prebreakdown channel may seem to contradict available experimental evidence [25], which suggests that dart leaders increase the channel temperature up to about 20 000 K before a subsequent return stroke ensues. However, in the limit that the simulation corresponds to a cross section of the channel very close to the ground, dart leader and return stroke fuse together. In other words, in this limit, the dart leader signature is seen as the initial portion of the return stroke current rise. Therefore, the simulations shown here should be interpreted as the channel transformation from the pre-dart leader channel to the return stroke. Walker and Christian [2] report that the dart leader and return stroke signature happen one frame (or 1.5 μs) apart in their recordings. Additionally, it should be noted that the data-driven conclusions in this article are biased by the small dataset used, i.e., only a single triggered flash with five return strokes. For this particular flash, the first return stroke does not seem to be very different from the subsequent ones, and the subsequent strokes do not seem to differ from one another. Additional work is required to refine the computational model [1], but the results presented here already show that carefully choosing the transport coefficients can help improve the agreement between calculations and measurements. The subsequent efforts should include the collection of more data, and extended comparisons between model and observations.

IV. Conclusion

In this work, we presented results of data-constrained simulations of the lightning return stroke channel plasma properties using the model proposed by da Silva *et al.* [1]. The simulations are constrained by the data collected by Walker and Christian [2], [3]. The model is driven by the measured channel-base current and the calculated temperature and electron density are compared to the respective measurements. Typical errors found are of the order of tens of percent. We discuss how replacing the transport coefficients from Boulos *et al.* [15] with the ones from D'Angola *et al.* [16] improves the agreement between model and data. The upgrade allows the model to approach the high electron densities measured. However, the highest electron densities calculated with the model are still one order of magnitude lower than the values derived from the experiment.

Upon establishing confidence in the model, we proceeded to tabulate important return stroke channel parameters that cannot be easily measured, such as radius, resistance, electric field, energy deposition (rate and magnitude), and more. Estimates on radius, resistance, and deposited energy are comparable to what has been previously published in the literature. The primary issue with comparing to what is available in the literature is that all plasma properties have an inherent dependence on the history of electrical current flowing through the channel. We circumvent this issue by reporting important parameters as a function of return stroke peak current and also at two different instants (or regimes): 1) at the instant of peak power and 2) 100 μs later (when the channel is fully established). These calculations are provided with the hope that they may be useful for applications aimed at quantifying the impacts of lightning in the atmosphere and, perhaps, to contribute to the validation of lightning discharge models aimed at the protection of our society's infrastructure.

REFERENCES

[1] C. L. da Silva, R. G. Sonnenfeld, H. E. Edens, P. R. Krehbiel, M. G. Quick, and W. J. Koshak, "The plasma nature of lightning channels and the resulting nonlinear resistance," *J. Geophys. Res.*, vol. 124, no. 16, pp. 9442–9463, Aug. 2019.

[2] T. D. Walker and H. J. Christian, "Triggered lightning spectroscopy: Part 1. A qualitative analysis," *J. Geophys. Res.*, vol. 122, no. 15, pp. 8000–8011, 2017.

[3] T. D. Walker and H. J. Christian, "Triggered lightning spectroscopy: 2. A quantitative analysis," *J. Geophys. Res.*, vol. 124, no. 7, pp. 3930–3942, 2019.

[4] V. A. Rakov and M. A. Uman, *Lightning: Physics and Effects*. Cambridge, U.K.: Cambridge Univ. Press, 2003.

[5] W. J. Koshak, R. J. Solakiewicz, and H. S. Peterson, "A return stroke NO_x production model," *J. Atmos. Sci.*, vol. 72, no. 2, pp. 943–954, 2015.

[6] A. De Conti, S. Visacro, N. Theethayi, and V. Cooray, "A comparison of different approaches to simulate a nonlinear channel resistance in lightning return stroke models," *J. Geophys. Res.*, vol. 113, 2008, Art. no. D14129.

[7] F. Rachidi, "A review of field-to-transmission line coupling models with special emphasis to lightning-induced voltages on overhead lines," *IEEE Trans. Electromag. Compat.*, vol. 54, no. 4, pp. 898–911, Aug. 2012.

[8] L. Chemartin *et al.*, "Direct effects of lightning on aircraft structure: Analysis of the thermal, electrical and mechanical constraints," *J. Aerosp. Lab.*, vol. 5, no. AL05-09, pp. 1–15, Dec. 2012.

[9] V. A. Rakov and M. A. Uman, "Review and evaluation of lightning return stroke models including some aspects of their application," *IEEE Trans. Electromag. Compat.*, vol. 40, no. 4, pp. 403–426, Nov. 1998.

[10] M. N. Plooster, "Numerical model of the return stroke stroke of the lightning discharge," *Phys. Fluids*, vol. 14, no. 10, pp. 2124–2133, 1971.

[11] A. H. Paxton, R. L. Gardner, and L. Baker, "Lightning return stroke. A numerical calculation of the optical radiation," *Phys. Fluids*, vol. 29, no. 8, pp. 2736–2741, Aug. 1986.

[12] R. E. Orville, "A high-speed time-resolved spectroscopic study of the lightning return stroke: Part I. A qualitative analysis," *J. Atmos. Sci.*, vol. 25, no. 5, pp. 827–838, Sep. 1968.

[13] R. E. Orville, "A high-speed time-resolved spectroscopic study of the lightning return stroke: Part II. A quantitative analysis," *J. Atmos. Sci.*, vol. 25, no. 5, pp. 839–851, Sep. 1968.

[14] R. E. Orville, "A high-speed time-resolved spectroscopic study of the lightning return stroke. Part III. A time-dependent model," *J. Atmos. Sci.*, vol. 25, no. 5, pp. 852–856, Sep. 1968.

[15] M. I. Boulos, P. Fauchais, and E. Pfender, *Thermal Plasmas, Fundamentals and Applications*. New York, NY, USA: Plenum, 1994, vol. 1.

[16] A. D'Angola, G. Colonna, C. Gorse, and M. Capitelli, "Thermodynamic and transport properties in equilibrium air plasmas in a wide pressure and temperature range," *Eur. Phys. J. D*, vol. 46, no. 1, pp. 129–150, Jan. 2008.

[17] Y. Cressault, R. Hannachi, P. Teulet, A. Gleizes, J.-P. Gonnet, and J.-Y. Battandier, "Influence of metallic vapours on the properties of air thermal plasmas," *Plasma Sources Sci. Technol.*, vol. 17, Aug. 2008, Art. no. 35016.

[18] M. Cho and M. J. Rycroft, "Computer simulation of the electric field structure and optical emission from cloud-top to the ionosphere," *J. Atmos. Solar-Terr. Phys.*, vol. 60, no. 7–9, pp. 871–888, 1998.

[19] G. G. Chernyi, S. A. Losev, S. O. Macheret, and B. V. Potapkin, *Physical and Chemical Processes in Gas Dynamics: Physical and Chemical Kinetics and Thermodynamics of Gases and Plasmas*, vol. 197. Reston, VA, USA: Amer. Inst. Aeronaut. Astronaut., 2004.

[20] J. A. Bittencourt, *Fundamentals of Plasma Physics*, 3rd ed. New York, NY, USA: Springer, 2004.

[21] J. T. Pilkey, "Rocket-triggered lightning propagation and North-Florida thunderstorm charge structure," Ph.D. dissertation, Dept. Elect. Comput. Eng., Univ. Florida, Gainesville, FL, USA, 2014.

[22] W. R. Gamerota, "The dart-stepped leader in rocket-triggered lightning," Ph.D. dissertation, Dept. Elect. Comput. Eng., Univ. Florida, Gainesville, FL, USA, 2014.

[23] V. Jayakumar, V. A. Rakov, M. Miki, M. A. Uman, G. H. Schnetzer, and K. J. Rambo, "Estimation of input energy in rocket-triggered lightning," *Geophys. Res. Lett.*, vol. 33, no. 5, 2006, Art. no. L05702.

[24] V. Cooray, "Power and energy dissipation in negative lightning return strokes," *Atmos. Res.*, vol. 149, pp. 359–371, 2014.

[25] R. E. Orville, "Spectrum of the lightning dart leader," *J. Atmos. Sci.*, vol. 32, no. 9, pp. 1829–1837, 1975.

Michael C. Taylor was born in Rio Rancho, NM, USA, in 2000. He is currently working towards a Bachelor of Science degree in physics at the New Mexico Institute of Mining and Technology (New Mexico Tech or NMT), Socorro, NM.

He has been an Undergraduate Research Assistant with NMT's Langmuir Lab since 2019. His research interests include lightning plasma physics and computational simulations.

Caitano L. da Silva received the Ph.D. degree in electrical engineering from Penn State University, State College, PA, USA, in 2015.

He has been an Assistant Professor of Physics with New Mexico Tech, Socorro, NM, USA, since 2018. His ongoing NSF CAREER project is focused on the development of physics-based, computationally-efficient, and data-constrained models for advancing the understanding of lightning and its impacts. He has authored more than 20 articles on the research topics of lightning, atmospheric electricity, plasma discharges, electrical coupling of atmospheric regions, transient luminous events, and waves in plasmas.

T. Daniel Walker received the Ph.D. degree in physics from The University of Alabama in Huntsville, Huntsville, AL, USA, in 2015.

He has been a part of a number of space-based lightning missions with NASA including the ISS-LIS instrument. His research interests include lightning spectroscopy and air-borne electric field studies.

Hugh J. Christian received the Ph.D. degree in physics from Rice University, Houston, TX, USA, in 1976.

He is a pioneer in lightning and thunderstorm research, specializing in the optical observation of lightning from space. He was the Principal Investigator of the optical transient detector (OTD) and the lightning imaging sensor (LIS), and a Chief Advocate and Designer of the geostationary lightning mapper (GLM). His work at NASA provided the first accurate measurements of global lightning activity. He was also instrumental as part of the Lightning Advisory Panel in setting Lightning Launch Commit Criteria for space-based missions.